Journal of Magnetism and Magnetic Materials 340 (2013) 120–126

Contents lists available at SciVerse ScienceDirect

Journal of Magnetism and Magnetic Materials

journal homepage: www.elsevier.com/locate/jmmm

The effect of the size of the system, aspect ratio and impurities concentration on the dynamic of emergent magnetic monopoles in artificial spin ice systems

Alejandro León*

Facultad de Ingeniería, Ejército 441, Santiago, Chile

ARTICLE INFO

Article history:
Received 21 August 2012
Received in revised form
18 February 2013
Available online 11 April 2013

Keywords:
Magnetic monopole
Spin ice
Aspect ratio

ABSTRACT

In this work we study the dynamical properties of a finite array of nanomagnets in artificial kagome spin ice at room temperature. The dynamic response of the array of nanomagnets is studied by implementing a "frustrated celular autómata" (FCA), based in the charge model and dipolar model. The FCA simulations allow us to study in real-time and deterministic way, the dynamic of the system, with minimal computational resource. The update function is defined according to the coordination number of vertices in the system. Our results show that for a set geometric parameters of the array of nanomagnets, the system exhibits high density of Dirac strings and high density emergent magnetic monopoles. A study of the effect of disorder in the arrangement of nanomagnets is incorporated in this work.

1. Introduction

Based on Dirac's prediction about the existence of magnetic monopoles, considering the quantization of the electrical charge [1], many research teams have attempted to find these monopoles [2], but their results have been inconclusive. Attention is currently directed at the study of elemental excitations in natural and artificial spin ice systems [3–6]. Excitations appear in natural systems that are equivalent to the magnetic monopoles connected by Dirac strings, which can be observed indirectly [1,7–9]. In artificial systems a pattern of magnetic nanoislands is created with lithographic techniques (with a square lattice or kagome lattice) equivalent to natural spin ice systems [10]. In the case of artificial spin ice systems, the nanoisland is arranged such that there is frustration to minimize dipolar interaction. This allows for designing geometries where emergent excitations are present, equivalent to the magnetic monopoles of natural spin ice systems. As well, with the artificial spin ice systems it is possible to visualize the configuration of magnetic moments directly with different microscopic techniques. This allows for their study at ambient temperature and the simulation of the behavior of natural spin ice systems [10–16]. Mól and colleagues [17] were the first to report the existence of magnetic monopoles and Dirac strings in systems of artificial spin ice. Since that date, many theoretical and experimental studies have been made in artificial spin ice systems [18–23]. Mengotti et al. [24] recently published the results of direct observations of emergent monopoles and associated Dirac strings. These results are the first direct confirmation of the reduction in the dimensionality of the system as a result of the frustration in the artificial spin ice system. Mengotti's work provides experimental evidence of reverse magnetization through the Dirac string avalanches that join monopole–antimonopole pairs. The same work provides results of Monte Carlo simulations that are in agreement with experimental results. The excellent work of Mengotti et al. [24] provides very valuable information about the dynamic of these elemental excitations and about nucleation and avalanches in reverse magnetization. Equally, many questions were raised that have lead to studying some aspects of the studied system by the authors of this work[24]. For example, it is expected that the formation of monopole–antimonopole pairs begins at the ends of the sample and that the strings advance toward the center. In the aforementioned report [24], only the central region of the array is shown, without the possibility of verifying the initial formation of the strings. Equally, the Monte Carlo simulations of these and other authors, considering infinite systems, are not very efficient when studying at the beginning of the reversion of magnetization. One of the central points of this paper is to introduce the use of cellular automata to the field of frustrated magnets. In this work, we study the effect of the aspect ratio and size of the system on the formation of Dirac strings. A study of the effect of disorder in the arrangement of nanomagnets is incorporated in this work. We considered the system as a finite array of magnetic nanoislands and took into account the possible disorder in the value of the nanoisland moments. The simulation is carried out using a determinist type of cellular automaton [25], which considers the coordination number of the elements of the grid. The interaction among the nanoislands is studied under the magnetic charge model and dipolar model.

* Tel.: +56 2 26762484
E-mail address: alejandro.leon@udp.cl

0304-8853/$ - see front matter © 2013 Elsevier B.V. All rights reserved.
http://dx.doi.org/10.1016/j.jmmm.2013.03.034

2. Magnetic nanoisland arrays and emergent monopoles

The system studied in this work is a magnetic nanoisland array in a hexagonal lattice. Fig. 1 shows a scheme of the magnetic bars arranged on the sides of a hexagon. Three nanomagnets converge in the vertices of the hexagons, as can be appreciated in Fig. 1. Geometrically, we can define two non-equivalent vertices in the hexagonal lattice, vertices A and B, respectively. The two non-equivalent vertices form the unit cell of the entire array. The cell is shown in red in Fig. 1. In the magnetic charge model, the charges are concentrated in these vertices. We define the magnetic charge in a vertex as −1, when two poles south and a north pole of the three nanomagnets that form the vertex converge. Equally, we define the magnetic charge as +1, when two poles north and a south pole converge in the considered vertex. Fig. 2 shows the array with an applied magnetic field. The upper left of Fig. 2 shows the array submitted to a field in the direction of the negative axis x. In the lower left of the figure the field is shown directed to the right. The nanomagnets with the x component of the magnetic moment directed to the left are represented by gray squares, and the nanomagnets with the x component from the magnetic moment directed to the right are represented by dark blue squares. When the sample is totally magnetized in directions $+x$ or $-x$, all the type A vertices have +1 (−1) charges, while all the B vertices have −1 (+1) charges. This can be seen in Fig. 2.

We suppose that we are under the condition of total magnetization, with the magnetic field directed to the left (upper left of Fig. 2). Under this condition, we define a positive and mobile monopole, if a nanomagnet converging in a class A vertex inverts its magnetic moment. The charge of vertex A goes from $q_A = -1 \rightarrow q_A^* = +1 \Longrightarrow \Delta q_A = +2$. If this is produced in a B type vertex, we define a negative monopole and would have $q_B = +1 \rightarrow q_B^* = -1 \Longrightarrow \Delta q_B = -2$, where q_A^* and q_B^* represent the charge of the vertex after the inversion and q_A and q_B represent the charges of the vertices A and B, respectively, in the their initial states. In this manner, when a nanomagnet inverts its magnetic moment, emerges a monopole–antimonopole pair. Fig. 3a–d shows the generation of a pair of mobile monopoles and their separation, giving rise to a Dirac string. If the three nanomagnets that converge in a vertex invert their moments, the condition $\Delta q_A = +2$ and $\Delta q_B = -2$, is also generated, but in this case the monopoles remain trapped and do not move through the sample (Fig. 3e).

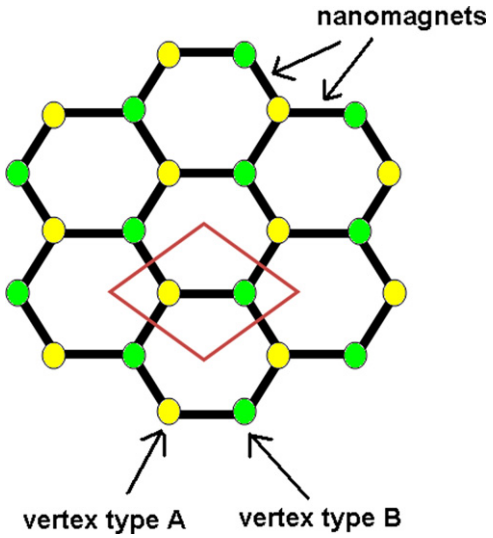

Fig. 1. Scheme of the nanomagnet array (black bars), vertices (yellow and green circles) and unit cell (in red). (For interpretation of the references to color in this figure legend, the reader is referred to the web version of this article.)

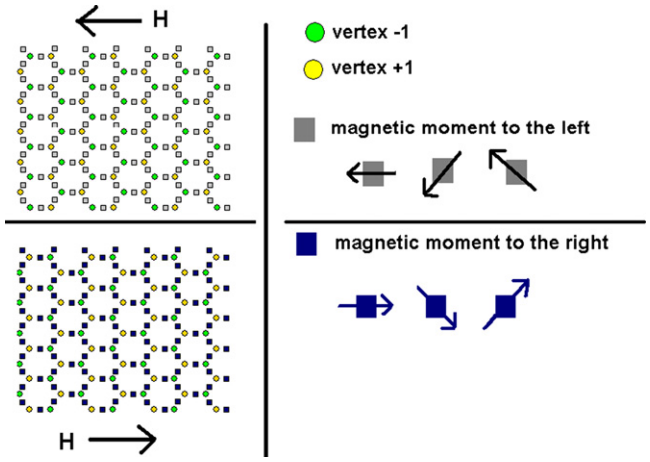

Fig. 2. Scheme of the nanomagnet array when the sample is totally saturated by the influence of an external magnetic field. (For interpretation of the references to color in this figure legend, the reader is referred to the web version of this article.)

3. Cellular automaton, the magnetic charge model and dipolar model

A cellular automaton (CA) is a mathematical structure used to model the dynamics of complex systems. It is formed by many simple entities that interact locally. A variety of models based on CA have been used to efficiently study problems in biology, physics, chemistry, engineering and material sciences [26,27]. They represent an excellent alternative to models based on differential equations and to Monte Carlo algorithms because they can simulate highly complex systems with a low computational cost. The first attempt to use CA in the study of magnetism was the model proposed by Vichniac [28], which was subsequently developed by Pomeau [29] and Hermann [30] and is termed the VPH model. This is being used to resolve an Ising type spin system. To avoid a "feedback catastrophe", the automaton is updated in more than one step. The model functioned well at high temperatures ($T > T_C$), but failed at low temperatures. Subsequently, Ottavi et al. [31] used a microcanonical algorithm in a CA to resolve the Ising spin system. A determinist version of this model provided acceptable results at a low temperature [31]. Owing to the popularity of the different types of Monte Carlo algorithms used in problems associated with spins, the development of CA models for these systems did not continue. In this work we used a CA model, different from previous models, developed specifically to resolve the dynamic of frustrated spins in artificial spin ice systems. This model allows the simulation of spin ice systems efficiently [25].

3.1. Frustrated cellular automaton (FCA)

This model was conceived for frustrated systems whose dynamic develops at zero temperature or the equivalent. In the case of artificial ice spin systems, each nanomagnet has a shape anisotropy with energy on the order of 10^4 K. This means that the thermal fluctuations in the configuration of moments are negligible at room temperature and consequently the system behaves like a system at zero Kelvin. To study this system in particular, we define the cells of the automaton in the vertices of the hexagonal structure. The ends of three nanomagnets converge in each vertex. Fig. 4a shows the structure of the FCA. The automaton is updated as follows:

1. A class of diagonal nanomagnets (d1 or d2) is randomly selected at each stage of the algorithm.

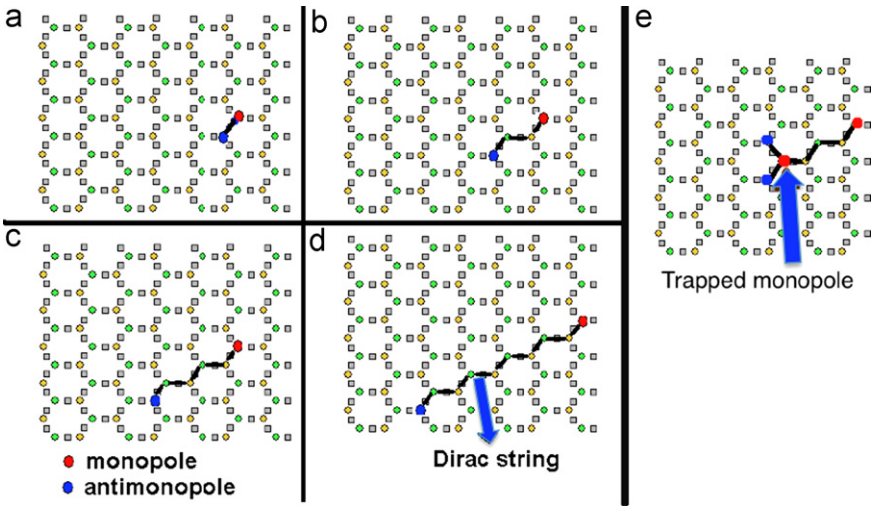

Fig. 3. Scheme of the creation of a monopole-antimonopole pair, the associated Dirac string and trapped monopole.

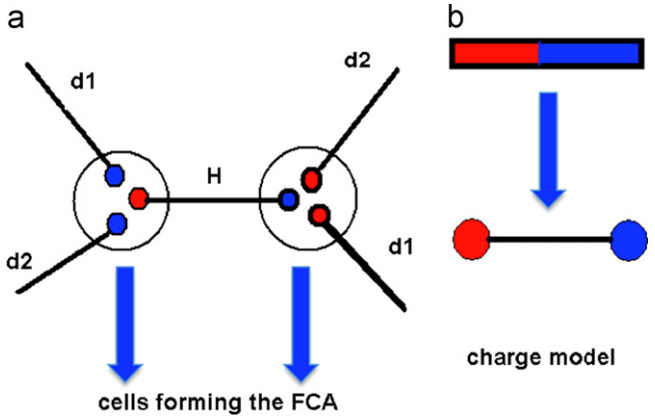

Fig. 4. (a) Scheme of the FCA cells. The horizontal nanomagnets will be labeled by H, and diagonals nanomagnets are labeled d1 and d2 respectively. (b) Scheme of replacing the magnetic moments by the magnetic charge model.

2. It covers all the vertices of the automaton.
3. The moment of the nanomagnet of the chosen class is inverted and if the total energy decreases (and this difference is greater than the energy barrier for investment), the change is accepted. The energy term is explained in the next paragraph. This new configuration is maintained in an auxiliary array.
4. The same is then done with the horizontal nanomagnet (H), not considering the nanomagnet of the non-selected class.
5. The auxiliary configuration is copied in the definite configuration and we return to step 1.

In this way, we study the dynamic of emergent monopoles with a deterministic model that allows studying finite systems, considering the effect of the edge and the size of the system on the dynamic. As well, it allows us to incorporate impurities in the sample and study the effect of these impurities in the monopoles and associated Dirac strings.

3.2. Magnetic charge model

The moment $\vec{m}$ of each nanoisland in this model is replaced by two charges (one positive and the other negative), located at the ends of the nanomagnet, as shown in Fig. 4b. The magnitude of each charge is $q=m/l$, where l is the length of the bar. The total charge in each vertex is the sum of the three charges associated with the vertex. Vertex j gives $Q_j=\sum_{k\epsilon j}q_k$. The total energy of the system is given by the expression:

$$U=\begin{cases}\frac{1}{2}\frac{\mu_0}{4\pi}\sum_{i,j}\frac{Q_iQ_j}{r_{ij}}, & i\neq j\\ f_i, & i=j\end{cases} \tag{1}$$

The term for $i\neq j$ takes into account the interaction among the vertices of the array. The term $i=j$ considers the energy of the site. This term considers the interaction among the ends of the three nanomagnets that converge. Fig. 5 shows a scheme of the configuration of charges in each vertex and the parameters of associated length.

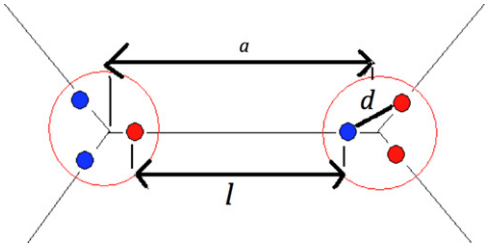

Fig. 5. Scheme of the configuration of charges in each vertex and of the length parameters. l represents the length of the nanomagnets, d represents the distance between the ends of two nanomagnets and a is the distance between two consecutive vertices. Furthermore al also corresponds to the hexagonal lattice parameter.

The energy in each vertex is given by the expression

$$f_i=\frac{\mu_0}{4\pi}\left\{\frac{q_1q_2}{d}+\frac{q_1q_3}{d}+\frac{q_2q_3}{d}\right\} \tag{2}$$

In accordance with the parameters of the hexagonal lattice $d=(\sqrt{3}/2)(a-l)$. Defining $q_0=m/l$ and writing the energy in units of $\mu_0q_0^2/4\pi a$, the total energy can be written as

$$U=\begin{cases}\frac{1}{2}\sum_{i,j}\frac{Q_iQ_j}{r_{ij}}, & i\neq j\\ \frac{2}{\sqrt{3}\varepsilon}\{q_1q_2+q_1q_3+q_2q_3\}, & i=j\end{cases} \tag{3}$$

With $\varepsilon=1-(l/a)$. When the automaton is updated, the change in total energy is registered (using Eq. (3)), that is, under the magnetic charge model. The interaction of the charges with the applied magnetic field is added to this term and the anisotropy energy term.

3.3. Dipolar interaction model

The dipolar interaction between sites on the kagome lattice is given by

$$U_{dip} = -\frac{\mu_0}{4\pi} \sum_{i,j(i\neq j)} \frac{1}{r_{ij}^3} \{3(\vec{m}_i \cdot \hat{r}_{ij})(\vec{m}_j \cdot \hat{r}_{ij}) - \vec{m}_i \cdot \vec{m}_j\} \quad (4)$$

where $\vec{m}_i = \alpha_i m \hat{e}_i$ is the magnetic moment at site i. Here the pseudospin $\alpha_i = \pm 1$ denotes the projection of the spin onto the anisotropy (local ising) directions $\hat{e}_i$ (directed along the links of the honeycomb lattice) and m is the magnetic moment of a nanoisland. The interaction of the charges with the applied magnetic field is added to this term and the anisotropy energy term.

4. Simulation and the results obtained

4.1. Monopoles and Dirac strings with the charge model and dipolar model

The first system studied, is a sample of (50 μm × 50 μm) and 5800 nanomagnets, with impurities. The lattice constant (the distance between two adjacent vertices) has a value of $a = 577$ nm. The random magnetic moment of individual islands is given by $m = m_0\beta$, where β is a dimensionless Gaussian random variable with $\langle\beta\rangle = 1$ and $s \equiv (\langle(\beta - \langle\beta\rangle^2)\rangle)^{1/2}$. In this first simulation, $s = 0.13$ and the energy barrier for the magnetic reversal is 98×10^4 kT, with T, the room temperature. This energy corresponds to a magnetic field of $\mu_0 H = 12,3\ mT$ used in the simulation Monte Carlo [24]. We define the number $f = monopoles/sites$, as the number of monopoles, for each vertex present in the system. We define the following physical observables: σ_M, as the number of mobile monopoles in units of the quantity f. N_T, as the total amount of monopoles, including monopoles mobile and non-mobile, in units of the quantity f. The magnetic field is shown as normalized to the coercive field H_C. Figs. 6 and 8 show the results of a single simulation. The purpose of working in this manner is to obtain the magnetic reversal in the nanomagnets (Figs. 7 and 9). In the rest of the graphics, the simulation is repeated 100 times. In these graphs (10, 11 and 12), we show the average value of the corresponding observable and its standard error. First, we do the simulation using the dipolar model. Fig. 6a shows the hysteresis curve, experimental data of the hysteresis curve [24] and the total density of monopoles. Fig. 6b shows the density of mobile monopoles and experimental data in function of the magnetic field. The agreement with experiment is very good. The discrepancy in the size of the hysteresis plateau between experiment and simulation is because in this region, this simulation is extremely sensitive to the sample considered. This means that our simulation of disorder in the sample, it is not very efficient in this region. This sensitivity is also reflected in the Monte Carlo simulation [24]. It is important to note that at the left end the sample ends with type "A" vertices and in the right end with type "B" vertices. The monopoles generated in the latter vertices, when the moments of the nanoislands are inverted are not mobile, and consequently cannot migrant through the sample. The latter implies that the pair generated in the ends only contributes a mobile monopole that is shifted toward the center of the sample because of the applied magnetic field. Fig. 7 shows a scheme of the complete sample (all the magnets) and the region that is considered for the statistical analysis (red rectangle), for values of the magnetic field near the coercivity. This figure does not include the color of each vertex to better appreciate the mobile monopoles. The impurities present in the sample (which were deposited randomly) produce mobile monopoles pairs in every region of the surface and both the positive and negative pole can move. This is clearly illustrated in Fig. 7, which simulates the dynamic of

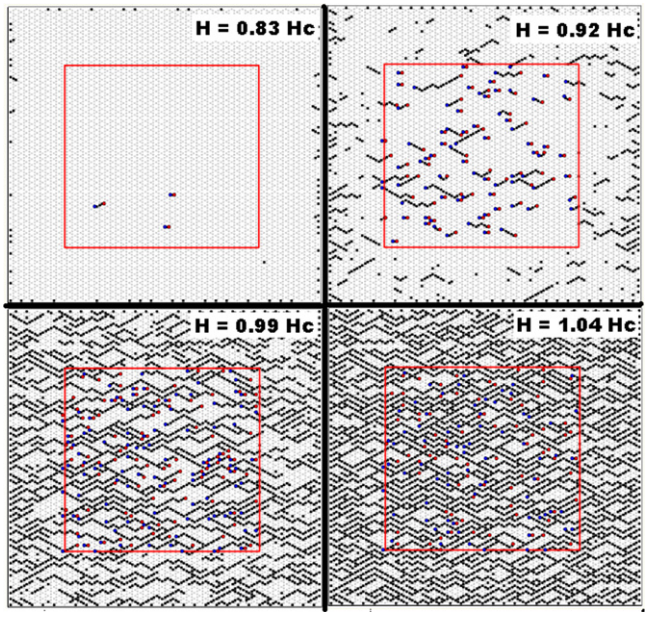

Fig. 7. Scheme of the simulation of the dynamic of monopoles and Dirac strings for a system with 5800 nanoislands (dipolar model). This simulation corresponds to the results showed in Fig. 6. (For interpretation of the references to color in this figure legend, the reader is referred to the web version of this article.)

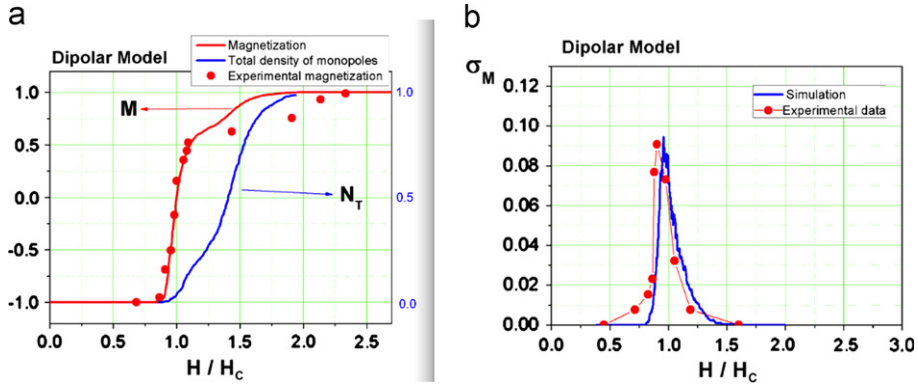

Fig. 6. Dipolar model ($\mu_0 H_c = 18.05$ mT). (a) Experimental hysteresis curve [24] (red points), simulated hysteresis curve (red line) and total density of monopoles (blue line). (b) Density of mobile monopoles (experiment [24] and simulation). (For interpretation of the references to color in this figure legend, the reader is referred to the web version of this article.)

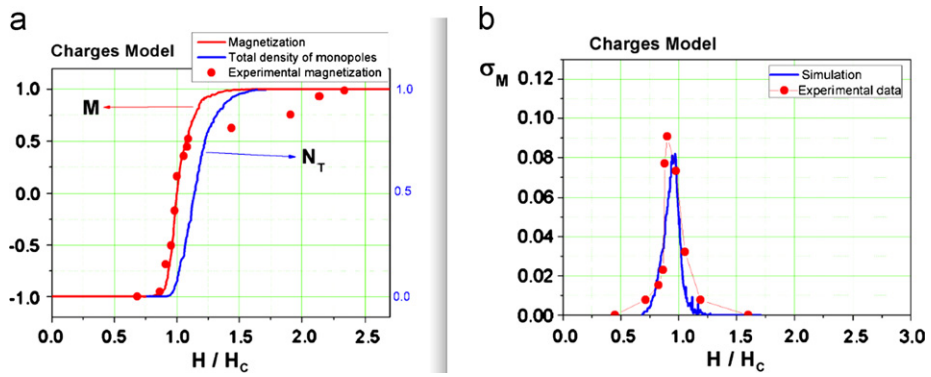

Fig. 8. Magnetic charge model ($\mu_0 H_c = 11.01$ mT). (a) Experimental hysteresis curve [24] (red points), simulated hysteresis curve (red line) and total density of monopoles (blue line). (b) Density of mobile monopoles (experiment [24] and simulation). (For interpretation of the references to color in this figure legend, the reader is referred to the web version of this article.)

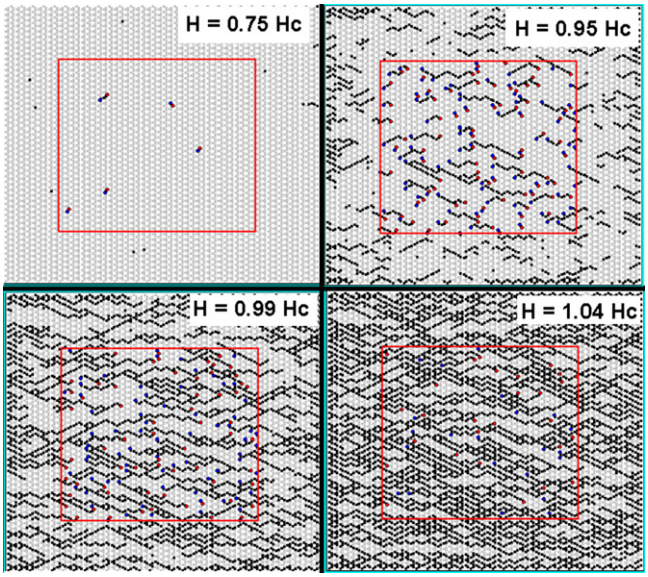

Fig. 9. Scheme of the simulation of the dynamic of monopoles and Dirac strings for a system with 5800 nanoislands (charge model). This simulation corresponds to the results showed in Fig. 8. (For interpretation of the references to color in this figure legend, the reader is referred to the web version of this article.)

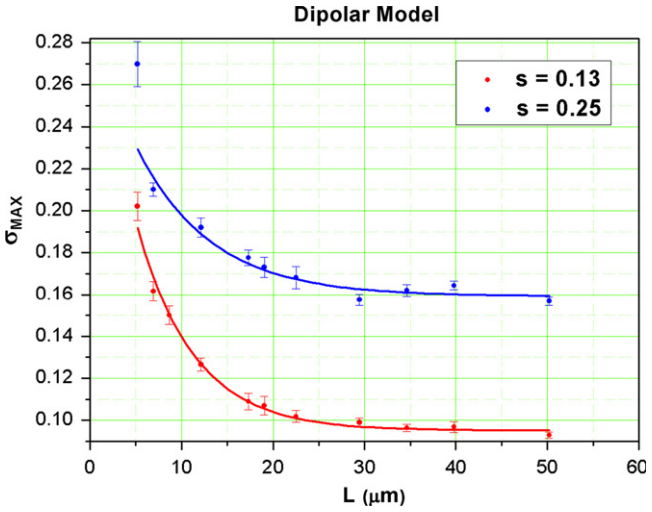

Fig. 10. Dependence of the density of the monopoles on the size of the system (dipolar model). The simulation is repeated 100 times and we show the average value of σ_{MAX} and its standard error. The blue curve shows the results for $s=0.25$ (high disorder) and the red curve shows the results for $s=0.13$ (low disorder). (For interpretation of the references to color in this figure legend, the reader is referred to the web version of this article.)

system. We can note that some pairs of emergent monopoles appears in the center of the sample. These emergent monopoles, which come from impurities and are generated in the central part of the nanomagnet arrays, move toward the ends, thus extending the Dirac string.

We now examine the behavior of the system using the magnetic charge model. All parameters are identical to the dipolar case, but now we add the size of the magnets (required in this model). We use the value $l=430$ nm, which allows us to obtain the experimental energy of site. Fig. 8a shows the hysteresis curve, experimental data of the hysteresis curve [24] and the total density of monopoles. Fig. 8b shows the density of mobile monopoles and experimental data in function of the magnetic field. We can appreciate some important differences compared to dipolar simulation. First, the maximum density of magnetic monopoles reaches a value of $0.082f$, compared to the value of $0.095f$ in dipolar simulation.

Moreover, the total density of monopoles presents a curve with a slope greater than in the case dipolar. The hysteresis curve has no plateau characteristic of experimental data and dipolar simulation. These differences in results are due to the energy of the site (charge model), which prevents the initial reversal of nanomagnets H (Fig. 4). This behavior can be seen by comparing Figs. 7 and 9.

We can appreciate a good agreement between the statistical results of the dipolar simulation with experimental statistical results. However, the images XMCD (X-Ray Magnetic Circular Dichroism) of the experimental paper in the first phase of magnetic reversal are more similar to the images obtained with the simulation of magnetic charges.

4.2. The effect of the size and aspect ratio of the system on the dynamic of emergent magnetic monopoles

We summarize our study of the density of mobile monopoles in function of the size of the system. For each size, the simulation was repeated 100 times. The error bars in the graphs correspond to standard error. Fig. 10 shows the maximum density of mobile monopoles, in units of f, using the dipolar model, for two concentrations of impurities $s=0.13$ and $s=0.25$. All systems, shown in Fig. 10, have square geometry. Axis x in Fig. 10 shows the side of the square in μm. From the figure, we can appreciate that for all systems, the density of the mobile monopoles is higher

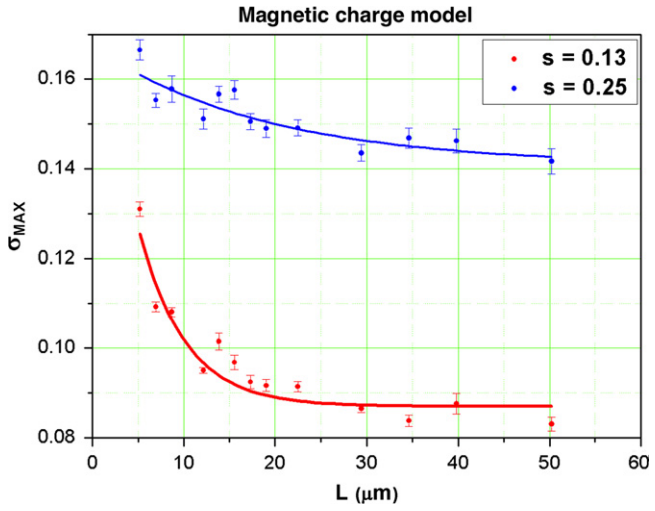

Fig. 11. Dependence of the density of the monopoles on the size of the system (charge model). The simulation is repeated 100 times and we show the average value of σ_{MAX} and its standard error. The blue curve shows the results for $s=0.25$ (high disorder) and the red curve shows the results for $s=0.13$ (low disorder). (For interpretation of the references to color in this figure legend, the reader is referred to the web version of this article.)

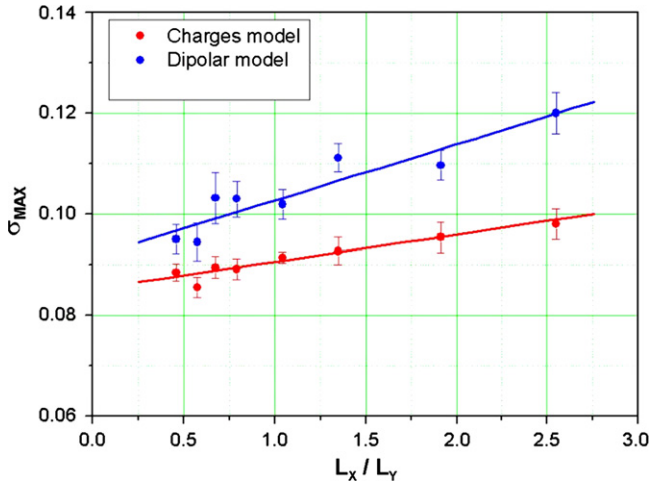

Fig. 12. Dependence of the density of the monopoles on the aspect ratio of the system. The simulation is repeated 100 times and we show the average value of σ_{MAX} and its standard error. The blue curve shows the simulation performed using the dipolar model. The red curve shows the results obtained with the charge model. In both simulations the parameter that measures the disorder in the sample has the value $s=0.13$.

for the case with $S=0.25$. As the size of the system decreases, the density with impurities approaches to the maximum value of the f. Our study verifies that the maximum density of magnetic monopoles decreases exponentially with system size. Fig. 11 shows the same studied, using charge model. We can verify a qualitative behavior similar to the dipole model, but with lower density values. (discrepancy explained above).

Finally, we show the results of the study considering the aspect ratio of the system. Fig. 12 shows the maximum value of the density of mobile monopoles in function of the ratio L_X/L_Y, where L_X is the length of the sample in the direction parallel to the magnetic field and L_Y is the direction perpendicular to the magnetic field. All systems studied have an impurity concentration, equivalent to $s=0.13$. Our results show that the density of mobile monopoles increases linearly with aspect ratio of the sample. The simulation based on the dipolar model shows a higher rate of change in the density of monopoles.

5. Conclusions

In this work we have studied the dynamic of magnetic monopoles emergent in an artificial spin ice system. An algorithm based on a frustrated cellular automaton was used in the magnetic charge model and dipolar model. The great advantage of the model is that it can make efficient simulations of highly complex phenomena in real time with a minimum of computational requirements. The model represents a perfect complement to the methods based on Monte Carlo algorithms to study the elemental physics of problems with classical and quantum entities. Our results show that the number of emerging magnetic monopoles depends of the sample size, the aspect ratio and the concentration of impurities. This allows us to consider a possible engineering in the creation of these systems for applications, for example in information technologies [32].

In a recent paper by Silva et al. [33], the authors studied the case where the system, in a square lattice, has one spin smaller (or greater) than the others. In their work, the authors show that two extreme points of the defect behave like a pair of magnetic monopoles. Their results are an important step towards understanding how lattice defects could change the thermodynamics of artificial spin ices [34]. It seems appropriate to continue this study on the dynamics of emerging monopoles in the presence of disorder, considering this new scenario from the results obtained by the study [33].

Acknowledgments

The author acknowledge the financial support of FONDECYT Program Grant 11100045.

References

[1] P.A.M. Dirac, Quantised singularities in the electromagnetic field, Proceedings of the Royal Society of London A 133 (1031) 60-72.
[2] K.A. Milton, Reports on Progress in Physics 69 (2006) 1637.
[3] C. Castelnovo, R. Moessner, S.L. Sondhi, Magnetic monopoles in spin ice, Nature 451 (2008) 42–45.
[4] O. Tchenyshyov, Magnetism: freedom for the poles, Nature 451 (2008) 22–23.
[5] L. Balents, Spin liquids in frustrated magnets, Nature 464 (2010) 199–208.
[6] H. Kadowaki, et al., Observation of magnetic monopoles in spin ice, Journal of the Physical Society of Japan 78 (2009) 103706.
[7] L.D.C. Jaubert, P.C.W. Holdsworth, Signature of magnetic monopole and Dirac string dynamics in spin ice, Nature Physics 5 (2009) 258–261.
[8] D.J.P. Morris, et al., Dirac strings and magnetic monopoles in spin ice $Dy_2Ti_2O_7$, Science 326 (2009) 411–414.
[9] T. Fennell, et al., Magnetic Coulomb phase in the spin ice $Ho_2Ti_2O_7$, Science 326 (2009) 415–417.
[10] R.F. Wang, et al., Artificial "spin ice" in a geometrically frustrated lattice of nanoscale ferromagnetic islands, Nature 439 (2006) 303–306.
[11] E. Mengotti, et al., Building Blocks of an artificial kagome spin ice: photoemission electron microscopy of arrays of ferromagnetic islands, Physical Review B 78 (2008) 144402.
[12] A. Remhof, et al., Magnetostatic interactions on a square lattice, Physical Review B 77 (2008) 134409.
[13] S. Ladak, D.E. Read, W. Branford, L.F. Cohen, New Journal of Physics 13 (2011) 063032.
[14] P. Mellado, O. Petrova, Y.C. Shen, O. Tchernyshyov, Physical Review Letters 105 (2010) 187206.
[15] S. Ladak, D. Read, Tyliszczak, W.R. Branford, L.F. Cohen, New Journal of Physics 13 (2011) 023023.
[16] S. Ladak, D. Read, G.K. Perkins, L.F. Cohen, W.R. Branford, Nature Physics 6 (2010) 359.
[17] L.A. Mól, R.L. Silva, R.C. Silva, A.R. Pereira, W.A. Moura-Melo, B.V. Costa, Journal of Applied Physics 106 (2009) 063913.
[18] J.P. Morgan, A. Stein, S. Langridge, C.H. Marrows, Nature Physics 7 (2011) 75.
[19] Z. Budrikis, J.P. Morgan, J. Akerman, A. Stein, P. Politi, S. Langridge, C.H. Marrows, R.L. Stamps, Physical Review Letters 109 (2012) 037203.
[20] S.A. Daunheimer, O. Petrova, O. Tchernyshyov, J. Cumings, Physical Review Letters 107 (2011) 167201.
[21] S.D. Pollard, V. Volkov, Y. Zhu, Physical Review B 85 (2012) 180402.

[22] R.V. Hügli, G. Duff, B. O'Conchuir, E. Mengotti, A.F. Rodríguez, F. Nolting, L.J. Heyderman, H.B. Braun, Philosophical Transactions of the Royal Society A 370 (2012) 5767.
[23] R.V. Hügli, G. Duff, B. O'Conchuir, E. Mengotti, L.J. Heyderman, A. Fraile Rodríguez, F. Nolting, H.B. Braun, Journal of Applied Physics 111 (2012) 07E103.
[24] E. Mengotti, et al., Real-space observation of emergent magnetic monopoles and associated Dirac strings in artificia kagome spin ice, Nature Physics 7 (2011) 68–74.
[25] A. León, An efficient model to study the dynamics of frustrated systems, Computer Physics Communications 183 (2012) 2089–2097.
[26] D. Griffeath, C. Moore (Eds.), New Constructions in Cellular Automata, University Press, Oxford, 2003.
[27] A. León, Z. Barticevic, M. Pacheco, Simulation of the first growth phase of single-walled carbon nanotubes using a model based on a cellular automaton, Solid State Communications 152 (2012) 41–44.
[28] G.Y. Vichniac, Physica D 10 (1984) 96.
[29] Y. Pomeau, Journal of Physics A 17 (1984) L-415.
[30] H.J. Hermann, Journal of Statistical Physics 45 (1986) 145.
[31] H. Ottavi, O. Parodi, Simulation of the ising model by cellular automata, Europhysics Letters 8 (1989) 741–746.
[32] M. Macucci, Quantum Cellular Automata, Imperial College Press, London, 2006.
[33] R.C. Silva, R.J.C. Lopes, L.A.S. Mól, W.A. Moura-Melo, G.M. Wysin, A.R. Pereira, Physical Review B 87 (2013) 014414.
[34] R.C. Silva, F.S. Nascimento, L.A.S. Mól, W.A. Moura- Melo, A.R. Pereira, New Journal of Physics 14 (2012) 015008.